Available online at www.sciencedirect.com

ScienceDirect

Procedia Structural Integrity 37 (2022) 299–306

Structural Integrity Procedia

www.elsevier.com/locate/procedia

ICSI 2021 The 4th International Conference on Structural Integrity

Quantitative Thermometry: A Revived Simplified Approach to Fatigue Strength Determination and Deformation Mechanisms

Florian Schäfer[a,*], Jan Rosar[a], Michael Marx[a], Franziska Herter[b], Haoran Wu[c], Peter Starke[c]

[a]*Materials Science and Methods, Saarland University, Campus D2 3, 66123 Saarbruecken, Germany*
[b]*Production Engineering, Saarland University, Campus A4 2, 66123 Saarbruecken, Germany*
[c]*Materials Science and Materials Testing, University of Applied Sciences Kaiserslautern, Schoenstraße 11, 67659 Kaiserslautern, Germany*

Abstract

It has long been known that plastic deformation and fatigue damage lead to a heat generation im metals. In the past two decades, thermographic approaches have been improved by thermography and widely adapted to obtain an estimate for the fatigue strength from the change in temperature or the amount of heat generation. In this study, based on a 40-year-old, but rarely established measurement technique using NTC thermistors, the temperature profile on a specimen was gathered and assessed based on state-of-the-art evaluation strategies, e.g., also by using infrared camera technology. A direct comparison with thermographic measurement not only reveals the significantly higher resolution of this simple and inexpensive method. It also elucidated that in the transition from low to high heat generation, associated with a lower estimate for the fatigue strength, for some groups of materials the high resolution of the NTCs is necessary for a reliable determination.

Keywords: Thermometry, Thermography; Fatigue Strength; Fatigue Strength Estimation; Fatigue Testing

1. Introduction

A simple and fast and hence cost-efficient method of acquiring an S-N curve has been one of the great challenges of materials testing for more than 100 years. Although it is already possible with short-time procedures such as the *PHYBAL*$_{\mathrm{LIT}}$ method, introduced by Starke et al. (2006), to obtain a S-N-curve in the finite-lifetime regime with only 3 specimens, the fatigue strength and thus the fatigue limit remains blurred. The Woehler test can only be successfully substituted if a simple method for determining the fatigue strength is available.

10.1016/j.prostr.2022.01.088

Since fatigue degradation of metals in the first half of the fatigue life is usually due to changes in defect structure and density, quantitative thermometry (QT) and fatigue testing were combined quite early by Stromeyer (2014). The underlying principle originates from the fact that e.g. dislocation motion leads to energy dissipation, which then manifests itself in a mechanical hysteresis and in heat generation and/or subsequently as a temperature increase near the middle of the specimen. The correlation of an onset of a temperature rise in the middle of the specimen with material damage has been investigated in a large number of studies, such as Luong (1998) and La Rosa and Risitano (2000). However, to approach the fatigue strength level, a closer look at the processes inside the material and gathering the resulting temperature distribution with maximal resolution is needed.

As early as 1982, Staerk (1982) was able to show that thermistors with negative temperature coefficients, so-called NTCs, can be used to achieve outstanding resolutions in temperature measurement at sampling points and thus in determining the temperature profile of the specimen that is directly linked to the heat generation originating from dislocation motion and interaction (Meneghetti (2007)). However, as thermography progressed, this method fell behind because thermography allows for a localized detection of failure although it is afflicted by a much lower accuracy.

Now, the aim of this study is to evaluate the limits of QT and if a thermographic acquisition of the temperature profile benefits from the larger number of sampling points as supposed by Guo et al. (2015). The limits are evaluated by a variety of materials with different thermal conductivity, different specimen geometries and underlying plastic deformation mechanisms.

2. Methods and Materials

2.1. Thermodynamic Background

Fatigue of metals is a dissipative process that can be described by quasi-static equations in the case of a steady state. Apart from a negligible portion, the work occurring as a mechanical hysteresis loop is dissipated in as heat, causing an increase of the temperature T in the process zone of the specimen tested. If a constant and isotropic thermal conductivity λ is assumed for a homogeneous isotropic material with constant mass density ρ and heat capacity C the one-dimensional heat equation becomes (Boulanger et al. (2004))

$$\rho C \frac{dT}{dt} - \lambda \frac{d^2T}{dx^2} = d_1 + s_{the} + s_{ic} + r_{ext} \tag{1}$$

The right-hand-side of Eq. (1) groups all the heat sources related to fatigue testing. $d_1(x,t)$ denotes the internal heat generation from dissipation, $s_{the}(x,t)$ is the heat generation from the thermoelastic effect and is not considered further because it vanishes when it is averaged for a sinusoidal load cycle. $s_{ic}(x,t)$ is the internal coupling source and expresses the heat generation by changes in the microstructure. It vanishes for fatigue testing a room temperature because for the metals tested here, the heat generation does not cause changes in the microstructure at the fatigue strength regime (at least this assumption is made for simplification). The external heat source $r_{ext}(x,t)$ is assumed to be time-independent and is vanishing therefore (Teng et al. (2020)). Hence fatigue of metals in the fatigue strength regime is considered as a purely dissipative process (Morabito et al. (2007)). In a steady state $\mathrm{d}T/\mathrm{d}t=0$ Eq. (1) simplifies to

$$d_1 + \lambda \frac{d^2T}{dx^2} = 0 \tag{2}$$

A polynomial solution with the curvature of the temperature profile and the heat generation rate $\dot{q}$ is given by

$$T(x) = -\frac{\dot{q}}{2\lambda} x^2 + mx + n \tag{3}$$

For at least 3 distinct sampling points x_i for the temperatures T_i the heat generated per load cycle q can be calculated by

$$q = \frac{\dot{q}}{f} = \frac{2\lambda}{f}\frac{(T_3-T_2)x_3-(T_2-T_1)x_1}{x_3x_1(x_3-x_1)} \tag{4}$$

regarding the test frequency f. Using 5 sampling points further improves the fit accuracy of the measured temperatures to the assumed parabolic temperature profile. This extension of the method is not part of this study because some of the tested specimens were too small for more than 3 NTCs.

2.2. Measurement of Temperature Profiles

Since the NTCs vary in their characteristic curve, the NTCs are calibrated in a water thermostat bath as shown in Fig. 1. For the characteristic curve the following equation is assumed and fitted to the data

$$T(R) = A + B\,ln\left(\frac{R}{R_0}\right) + C\,ln\left(\frac{R}{R_0}\right)^2 + D\,ln\left(\frac{R}{R_0}\right)^3 \tag{5}$$

with R being the electric resistance and R_0 being the reference value of the electrical resistance at 298 K. The high gradient of the $T(R)$ curve reveals the outstanding resolution of NTCs in combination with the resistance measurement using digital multimeters in the 10^{-5} K range.

In the fatigue strength regime, the heat generation is low and therefore the rise of the temperature too. Hence, the characteristic curve given in Eq. 5 can be linearized by a Taylor approximation. The error in measurement stays below 5 % until the onset of a severe temperature rise. The same error occurs because of the assumption that λ stays constant if the temperature increases. This error was also shown by Staerk et al. (1982) to stay below 5 % if the temperature increase stays below 30K and even lower if the increase is lower.

The NTCs are applied to the specimens as an array in a layered composite that allows an easy re-usage of the NTCs for several tests because the calibration is a time-consuming step before measurement (Fig. 2).

Stepwise load increase tests (LITs) were performed using a resonance testing device Rumul Mikrotron from Russenberger Pruefmaschinen AG, CH-Neuhausen am Rheinfall. The stress ratio R was varied between 0.1 and -1 to account for effects of reversible and non-reversible loading. The electrical resistance of the NTCs, type GAGA10KM3499J15 from TE Connectivity, were monitored using Keithley Digital Multimeters DMM 199 and the data acquisition was done using LabVIEW®. The raw data analysis was done with MATLAB®.

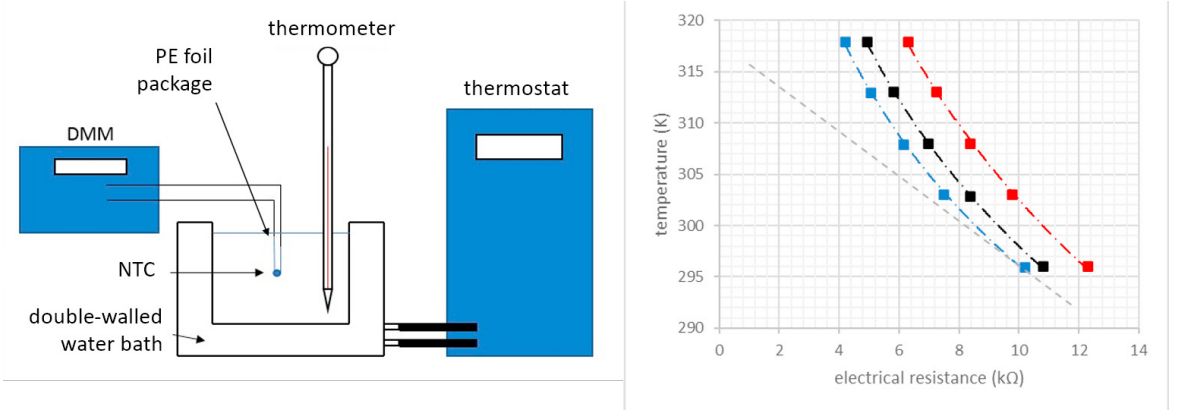

Fig. 1. Schematic of the setup for calibration of NTCs: The NTC is set to a thermostat bath inside a PE foil package and the bath temperature is varied and monitored by high-precision thermometers. The calibration curves for 3 different NTCs are shown on the right-hand side with a linear Taylor approximation at 298 K.

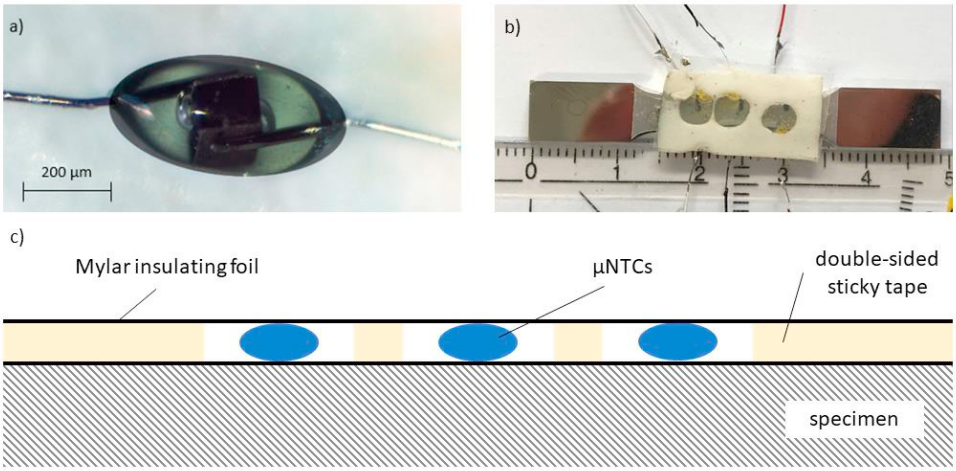

Fig. 2. a) Miniature axial loading NTC from TE Connectivity with Pt/Ir leads and fast response (< 1s), b) application of NTC array to Ni specimen, c) schematic of NTC array between Mylar insulating foil to avoid a short circuit and double-sided sticky tape to stabilize the re-usable setup.

All tests were performed at room temperature in a non-air-conditioned laboratory. An increase in the room temperature is not expected to influence the results because the temperature of the specimen mountings and the surrounding should not affect the accuracy of the measurement of the heat generated per load cycle as the curvature of the temperature profile is in the steads state. If the temperature difference between the mountings is well below the temperature rise in the middle of the specimen, no additional tempering is necessary. Besides these reflections, the specimens were isolated from their surrounding by a polyurethane pipe isolation, used for round specimens, and polystyrene plates, used for flat specimens.

Starting a new load step in the LIT, the specimen temperature in the middle of the process zone initially rises rapidly. After several load cycles, depending on the material's thermal conductivity and the amount of heat generation, a steady state temperature profile curvature is reached, and the calculated q from the NTC temperature measurements T_i is attributed to this load step amplitude σ_a.

2.3. Materials

For the fatigue tests, macro-round unnotched specimens were prepared from the non-alloyed carbon steels S235JR (1.0038) and 1.0314 and as well as flat specimens from nickel (Ni) (nanocrystalline (nc) and coarse-grained annealed (cg)), S235JR and $AlSi_{10}Mg$. The $AlSi_{10}Mg$ specimens were additively manufactured by selective laser melting (SLM) in three different orientations (0°, 45° and 90° relative to the layer normal). All specimen geometries were designed referring to ASTM standard E466-07 with a total length of 50 mm for the flat specimens and 87.5 mm for the round specimens. The parallel length on which the NTCs were applied were 10 and 15 mm, respectively.

The S235JR steel is used to verify the effect of different R ratios and the influence of specimen geometries (round and flat) whereas the 1.0314 steel is used to compare the fatigue strength estimated through QT with reference data evaluated in staircase tests as well as an estimate with the maximum-likelihood and the Hueck method. $AlSi_{10}Mg$ shows a very high thermal conductivity and low ductility. Hence, it is predominated to check for the limits of the method. The comparison between nc and cg Ni is used to reveal the effect of different deformation mechanisms on the heat generation per load cycle. Cg Ni deforms plastically by dislocation slip and interaction whereas nc Ni is known to deform by grain boundary-related mechanisms such as grain rotation, boundary sliding and dislocation interaction with the grain boundaries.

The specimens where carefully grinded and polished on all surfaces, finally with 1 µm diamond suspension, to avoid artefacts due to the condition of the specimen surface.

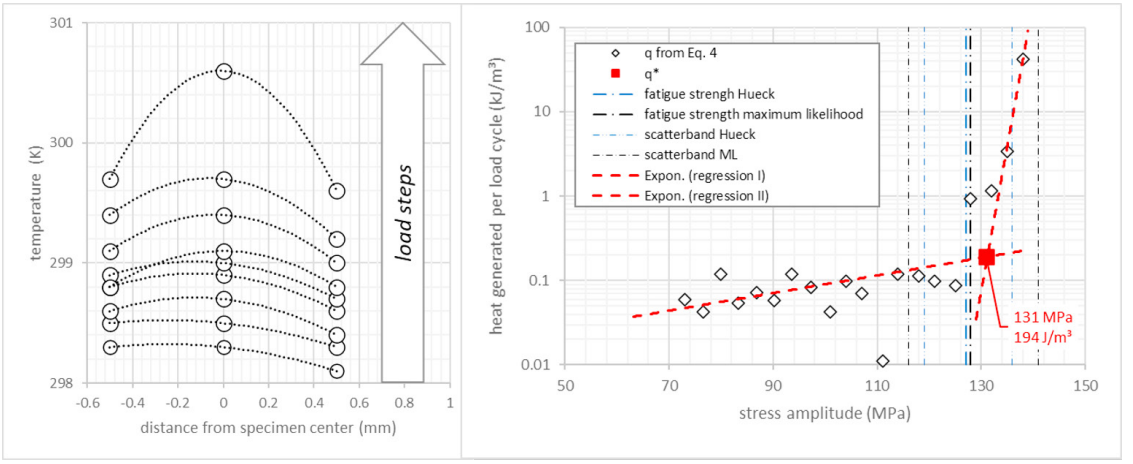

Fig. 3. Evolution of the measured temperature and estimated temperature profiles (Eq. 3/4) for the steady states of selected load steps (left-hand side); heat generated per load cycle q calculated with Eq. 4 from measured steady state temperature for 1.0314 steel at R=-1: The knee-point is evaluated by an iterative linear partwise regression from both sides of the dataset. The fatigue strength estimates from the staircase tests analyzed by the maximum likelihood and the Hueck method are added with their corresponding scatter bands (right-hand side).

3. Results

When the specimen is subjected to fatigue testing in a stepwise LIT, as mentioned above, an equilibrium temperature is developed at each load step after a certain number of load cycles due to the balance of heat generation from dissipation and heat loss via conduction. The time to reach this equilibrium can vary and depends primarily on the material and its physical parameters as well as on the individual cyclic deformation behavior characterized by cyclic softening and/or hardening, which in turn is mostly related on the heat treatment condition. The steady state quantity of heat per load cycle increases with increasing stress amplitude, which is evident by the increasing curvature of the temperature profile (Fig. 3). The curvature is calculated by Eq. 4 using three interpolation points from the temperature measurement at the three measuring points on the specimen.

If the steady state temperature profile with the corresponding heat quantity per load cycle q is juxtaposed to the stress amplitude at the corresponding load level, a characteristic curve is obtained as shown in Fig. 3 (right). These characteristic σ_a-q-plots are shown in Fig. 4 for the Al cast alloy AlSi10Mg from SLM and for the cg and nc Ni. Fig. 5 compares S235JR steel specimens tested at different R ratios and with different specimen geometry, whereas there is no evidence that the latter influences the test results.

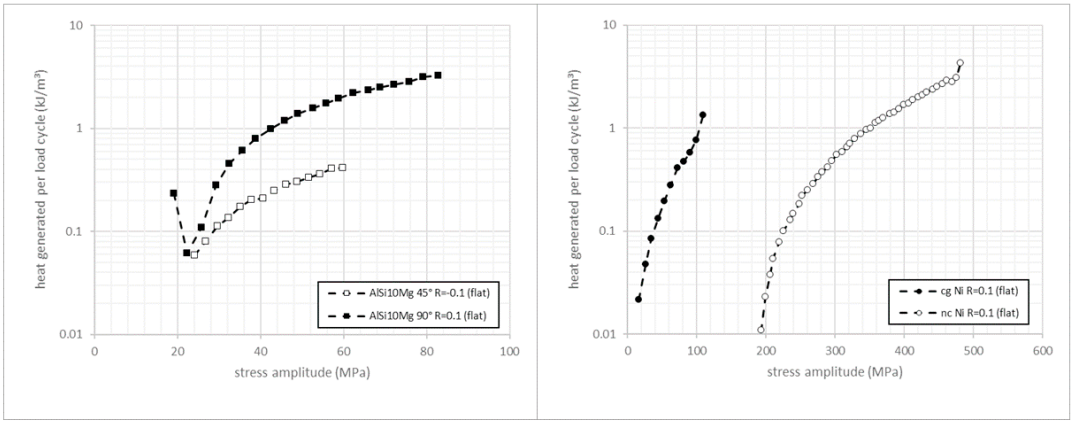

Fig. 4. Heat generated per load cycle for steel $AlSi_{10}Mg$ depending on the stress amplitude (left hand side) and for cg and nc Ni (right hand side).

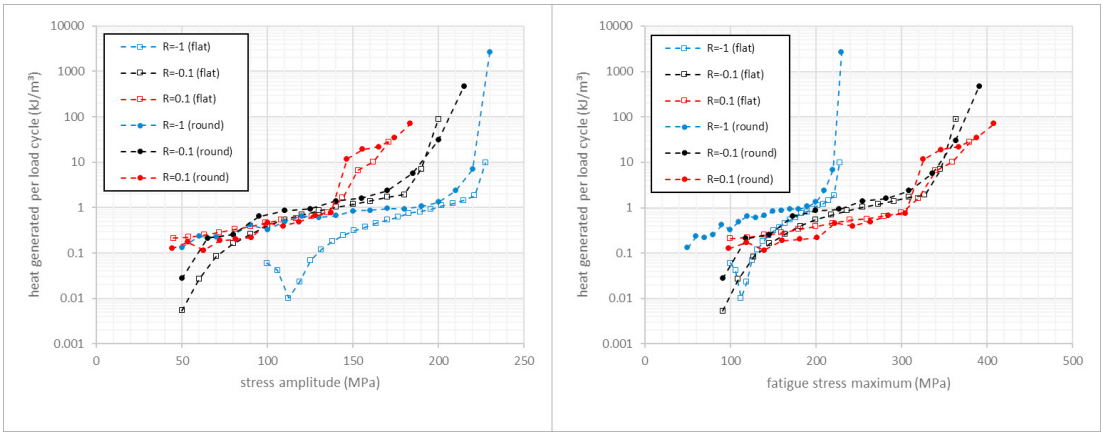

Fig. 5. Heat generated per load cycle for steel S235JR (1.0038) depending on the stress amplitude (left hand side) and the maximum stress (right hand side). The onset of heat generation is comparable for all R values whereas for R=0.1 the onset of plasticity results in a jump in the heat generation because dislocation motion starts immediately if the upper yield strength is reached, and the material softens. There is no evidence for a dependency of the results from the specimen geometry.

4. Discussion

4.1. The Knee-Point in the σ_a-q-plot as an Estimate of Fatigue Strength?

It is evident from the semi-logarithmic plot that the knee point in Fig. 3 (right) is accompanied by a transition of the cyclic strain hardening exponent according to Morrow et al. (1964) (Starke et al. (2006)). The strain hardening exponent below the knee point stress amplitude σ_a* is significantly below that above. The knee point is related to the onset of pronounced dislocation motion during cyclic deformation. This is particularly indicated by the fact that at a stress amplitude exceeding the upper yield strength, the S235JR steel shows a jump in the generated heat (Fig. 5), which is associated with the onset of massive dislocation motion with the softening.

Heat is also already generated below the knee point, but the amount of heat is comparable small. Mareau et al. (2012) attributed the energy dissipation in this range to anelastic effects such as a Snoek effect, the Zener mechanism, or dislocation oscillations. Maquin et al. (2009) explain the temperature increase is by the emission of acoustic waves during dislocation oscillation. In the range of high Morrow exponents, i.e., in the finite-lifetime regime, the high energy dissipation occurs due to dislocation motion, which in the end leads to damage (Connesson et al. (2011)).

Thus, the knee point stress amplitude σ_a* can be identified as a lower estimate of the fatigue strength and q* as the characteristic heat rate that shows, like a fingerprint, when dislocation motion starts. In this context, the level of q* is characteristic for each material. Comparing the knee point stress amplitude with conventionally obtained fatigue strength data according to Hueck or the maximum likelihood method (Fig. 3), the results of the QT are in very good agreement with the conventional determination of the characteristic values of the fatigue strength and the fatigue limit, respectively.

4.2. Influence of Specimen Geometry on QT Results?

The direct comparison in Fig. 5 for the S235JR steel from flat and round tensile specimens shows a well agreement between the curves for all testes R ratios. Thus, there is no evidence for an effect of the specimen geometry on the results. This further proves the high accuracy and the reliability of the QT method using NTCs.

4.3. Limits of the Method: High Thermal Conductivity and Low Ductility?

It is not trivial to specify a noise level for a measurement method that is based on the curvature of a discrete sampled value that additionally is not constant over time. However, it is clear from Fig. 3 that for those steps below q* the

values for q scatter about 0.1 kJ/m³. In the data from Fig. 4, it is also obvious that the characteristic σ_a-q-curve only becomes exponential if $q > 0.2$ kJ/m³ (linear in the semi-logarithmic plot). Therefore, the assumption that the method shows a minimum resolution of 0.1 kJ/m³ with a limit for a valid determination of heat generated per load cycle of 0.2 kJ/m³ is derived.

For example, considering a measurement length of 10 mm with 3 sensors and a test frequency of about 200 Hz in the resonance tests, this corresponds to a temperature resolution of 5 mK for a ferritic steel with a thermal conductivity assumed to be 50 W/(Km). However, the resolution of the QT method scales with $1/\lambda$, the test frequency f and the distance between the measurement points Δx and of course with the measurement accuracy of the temperature. Hence, the applicability of the method with the Al cast allow $AlSi_{10}Mg$ was validated. It is obvious, that when the cyclic yield strength is exceeded, failure immediately occurs. There is no evidence for a cyclic hardening above q^*. Although the effort of a QT measurement is not efficient for such a brittle material, the outstanding resolution of the QT method below q^* is shown in Fig. 4.

Another challenge of the method is that an equilibrium state must be reached. If this is omitted, the σ_a-q-plot forms a curvature below q^* as seen in Fig. 5 for the R = -1 flat specimen. This test was executed with just 10^4 instead of 10^5 load cycles at each step during the LIT. Nevertheless, the knee-point (σ_a^*,q^*) is reproduced clearly. Thus, it is expected that even a continuous load increase provides the same results as stepwise LITs.

4.4. QT and dominant Deformation Mechanism

Nc Ni responds to cyclic deformation with higher frequencies and thus higher strain rates in an embrittled manner because it exhibits a high strain rate sensitivity due to the necessity of dislocations interacting with grain boundaries as an essential deformation mechanism. The plastic deformation mechanism of nc Ni differs from the simple dislocation motion that the other materials exhibit after passing the knee-point. Hence, it is not clear if an expected exponential increase of q below q^* is easily transferrable to the complex deformation mechanisms in a nc material with a non-vanishing amount of microplasticity and time-dependent deformation mechanisms.

For cg Ni, it must be noted, that the dislocation motion already started during the first load cycle because the yield stress is below 5 MPa in the cg state. For cg f.c.c. materials, it is commonly known that a steady state is not reached until a complex fatigue dislocation structure is established and that this steady state is just present until crack initiation in persistent slip bands starts (Schaefer et al. (2017)).

As a result, the knee-points at the penultimate datapoints in Fig. 5 for the cg and the nc Ni specimen are not attributed to the onset of dislocation motion but to the initiation of cracking. For the nc material, the onset of cyclic plasticity is not revealed by the QT method. Plastic deformation seems to start continuously or/and with overlaid grain boundary-related deformation mechanisms.

5. Conclusion

Quantitative thermography, which uses discrete temperature sampling measured with NTCs to determine the curvature of the temperature profile of a metallic specimen, assumed to be parabolic, has been revived. The determined knee stress amplitude, obtained by comparing the applied stress amplitude and the heat generated per load cycle, was found to be a lower estimate of fatigue strength. The heat generated per load cycle at the knee point was found to be characteristic; a fingerprint of the heat rate associated with the onset of cyclic dislocation motion characteristic of a material and/or deformation mechanism.

The limitations of the method have been demonstrated using a variety of materials and load ratios. The method benefits from the excellent resolution of the NTCs. In addition, the method is simple and cost effective.

If it became possible to combine QT with short-time methods to evaluate the finite life fatigue regime, future research could determine a complete SN curve in a single specimen experiment.

Acknowledgements

We thank Marc Schmidt from the Technical University Kaiserslautern for providing the data for the fatigue strength of the material 1.0314 during his master thesis at FuWe of Saarland University. We acknowledge the financial support from Saarland for the resonance testing machine (DFG INST 256/500-1 LAGG) and the financial support from Deutsche Forschungsgemeinschaft and Saarland for the SLM machine in the State Major Instrumentation program with the reference INST 256/503-1 FUGG.

References

Boulanger, T., Chrysochoos, A., Mabru, C., Galtier, A., 2004. Calorimetric analysis of dissipative and thermoelastic e ects associated with the fatigue behavior of steels. International Journal of Fatigue 26(3), 221–229.

Connesson, N., Maquin, F., Pierron, F., 2011. Dissipated energy measurements as a marker of microstructural evolution: 316L and DP600. Acta Materialia,59(10), 4100-4115.

Guo, Q., Guo, X., Fan, J., Syed, R., Wu, C., 2015. An energy method for rapidevaluation of high-cycle fatigue parameters based on intrinsic dissipation. International Journal of Fatigue 80, 136–144.

La Rosa, G., Risitano, A., 2000. Thermographic methodology for rapid deter-mination of the fatigue limit of materials and mechanical components, International Journal of Fatigue 22(1), 65–73.

Schaefer, F., Lang, E. P., Bick, M., Knorr, A. F., Marx, M., & Motz, C., 2017. Assessing the intergranular crack initiation probability of a grain boundary distribution by an experimental misalignment study of adjacent slip systems. Procedia Structural Integrity 5, 547-554.

Luong, M. P., 1998. Fatigue limit evaluation of metals using an infrared thermo-graphic technique, Mechanics of materials 28(1-4), 155–163.

Meneghetti, G., 2007. Analysis of the fatigue strength of a stainless steel based on the energy dissipation, International Journal of Fatigue 29(1), 81–94.

Maquin, F., Pierron, F., 2009. Heat dissipation measurements in low stress cyclic loading of metallic materials: From internal friction to micro-plasticity. Mechanics of Materials 41(8), 928-942.

Mareau, C., Favier, V., Weber, B., Galtier, A., Berveiller, M., 2012. Micromechanical modeling of the interactions between the microstructure and the dissipative deformation mechanisms in steels under cyclic loading. International Journal of Plasticity 32, 106-120.

Morrow, J., 1965. Cyclic plastic strain energy and fatigue of metals. In Internal friction, damping, and cyclic plasticity. ASTM International.

Morabito, A., Chrysochoos, A., Dattoma, V., Galietti, U., 2007. Analysis of heat sources accompanying the fatigue of 2024 t3 aluminium alloys, International Journal of Fatigue 29(5), 977–984.

Staerk, K.F., 1982. Einsatz von Heißleitertemperaturfuehlern in der Werkstoffpruefung, Materialwissenschaft und Werkstofftechnik 13(9), 309–313.

Staerk, K.F., 1982. Temperaturmessung an schwingend beanspruchten Werkstoffen, Materialwissenschaft und Werkstofftechnik 13(10), 333-339.Starke, P., Walther, F., Eifler, D., 2006. PHYBAL—A new method for lifetime prediction based on strain, temperature and electrical measurements. International Journal of Fatigue 28(9), 1028-1036.

Stromeyer, C. E., 1914. The determination of fatigue limits under alternating stress conditions. Proceedings of the Royal Society of London. Series A, Containing Papers of a Mathematical and Physical Character 90(620), 411-425.

Teng, Z., Wu, H., Boller, C., Starke, P., 2020. Thermography in high cycle fatigue short-term evaluation procedures applied to a medium carbon steel, Fatigue & Fracture of Engineering Materials and Structures 43(3), 515–526.